ESRF	**Experiment title:** Origin of the drop in fatigue performance of transforming superelastic NiTi wires studied through spatially resolved in-situ x-ray microdifraction	**Experiment number**: MA-2880
Beamline: ID11	**Date of experiment**: from: **24 March 2016** to: **28 March 2016**	**Date of report**: 5th of August 2016
Shifts: 12	**Local contact(s)**: Nicholas Harcker	*Received at ESRF:*

Names and affiliations of applicants (* indicates experimentalists):

E. Alarcon Tarquino[1,2] *, L. Heller[2]*, L. Saint-Sulpice[1]*, S. Arbab Shirani[1]

1. France ENI Brest, FRE CNRS 3744, IRDL, F-29(200)M Brest, France

2. Institute of Physics, Academy of Sciences of the Czech Republic, 182 00 Prague, Czech Republic

High energy synchrotron radiation diffraction experiments were performed on medical-graded NiTi samples, which show superelastic behavior as a consequence of stress-induced martensitic transformations.

In the first part of this experimental campaign we tracked the martensitic transformation in hourglass-shaped samples (Fig.1a) where the transformation is triggered within a well-defined and localized gauge volume. Using these samples we could track the initiation of stress-induced transformation and deformation processes in martensite upon further loading. Furthermore, we investigated microstructure changes in hourglass-shaped samples due to various fatigue loadings that were applied ex-situ.

In the second part of this experimental campaign we investigated consequences of a notch in a superelastic ribbon (Fig.2a) to the course of the martensitic transformation and microstructure changes during superelastic cycling. When a superelastic component with geometric defects such as cracks or notches undergoes complete superelastic cycles, the martensitic transformation is inhomogeneous; it is first triggered at stress concentrating notches or cracks and then propagates to the rest of the sample. This inhomogeneous course of transformation may influence the crack growth and fatigue endurance of components containing geometric stress raisers.

Materials and Experimental protocol

Hourglass-shaped and notched ribbon samples were produced from 50.92 at. % Ni medical-graded NiTi. Hourglass shaped samples' geometry was obtained by grinding and electropolishing of 1.78mm diameter wires followed by annealing at 500°C for 30 min. Notched ribbon samples geometry was obtained by Electrical Discharge Machining of 0.1mm thick NiTi ribbons previously annealed at 450°C for 30 min. Samples were tested at room temperature (~24°C) using a stress rig , the tensile axis of which was aligned with the rotation axis of the platform of the diffractometer at the beamline ID11 at the ESRF (Fig 1b). We used a 5μm size monochromatic beam with energy equal to 65.38KeV resulting in wavelength of 0.189Å. The distance between the sample and the 2D detector was ~250mm allowing a maximal diffraction angle 2θ equal to 16°. The alignment of the stress rig and microscope platform axes facilitated the positioning of the sample with respect to the beam at different rotational angles (ω). This was especially important for verifying the assumption of axisymmetry of deformation states, stress induced martensite zone, and microstructure changes. After assuring correct positioning and alignment, samples were elongated in the axial direction (+z) until reaching a desired value of nominal tensile stress (F_z/A with A being the mid-cross section). Then, a series of scans were carried out while tensile stress magnitude was kept constant. Diffractometer movement allowed us to acquire series of vertical (z) and horizontal (y) 5μm spaced scans through the gauge volume of hourglass-shaped samples and 3μm spaced scans around the notch of notched ribbons samples. The acquisition time of 1s was used for each 2D diffraction pattern. For the first simplified data analysis, each 2D diffraction pattern was fully integrated and normalized using the Fast Azimuthal Integration algorithm provided by the software package pyFAI. It allowed rough spatially resolved inspection of acquired data on site during the experiment. The inspection was focused on the spatial distribution of austenite and martensite phases at different stages of loadings and for various loading histories. The simplified phase analysis was based on the evaluation of changes in the maximum profile intensity of dominant peaks $(110)_A$ and $(200)_M$ of the austenite and martensite phase, respectively. Microstructure changes and extent of retained martensite accumulated during cyclic loadings were also in the focus. These effects were evaluated so far qualitatively only by comparing diffraction patters of virgin samples with those acquired in unloaded state on samples that had undergone different number of cycles.

Results

Fig.1c and Fig.1d show the evolution of 1D diffraction patterns with nominal stress at the mid-cross section of a virgin hourglass-shaped samples. Results are presented in terms of diffraction patterns normalized to integrated intensity of the whole patterns. The strongest peak of $(110)_A$ plane of the B2 austenite phase appears in unloaded state (Fig.1d a.) while it splits into two peaks of trigonal R-phase induced by lower stresses (Fig.1b-f). At higher stress B19' martensite phase is induced (Fig.1d g.). The martensite phase formed instantaneously when reaching a critical stress level of 365 MPa in mid-cross-section. It appeared within a confined volume evaluated by scanning along the axis of the sample and evaluating maximum profile intensity of $(200)_M$ peak (Fig. 1e). The transformation event during

displacement controlled tensile loading was followed by a drop in tensile stress down to 350 MPa as seen in Fig. 1c.. The diffraction pattern of a virgin sample was considered as a reference to assess the fatigue damage accumulated after various fatigue loadings applied ex-situ. Fig. 1f,g presents comparisons of the reference pattern with the pattern measured on a sample that had been cycled 1000 times between 93.5 and 935MPa at 80°C, resulting in a very advanced fatigued state of approximately 90% of fatigue life. Comparison of patterns in unloaded state show very little changes (Fig. 1f) proving that the fatigue damage is highly localized into few fatigue cracks one of which was identified by diffraction patterns in loaded state below the martensitic transformation regime. In fact, scans along the axis near the surface combined with rotations discovered specific scanning positions at which martensite $(200)_M$ peaks appears (Fig. 1g) while most of patterns presented the R-phase. Martensite might be triggered by stress concentration at crack tips.

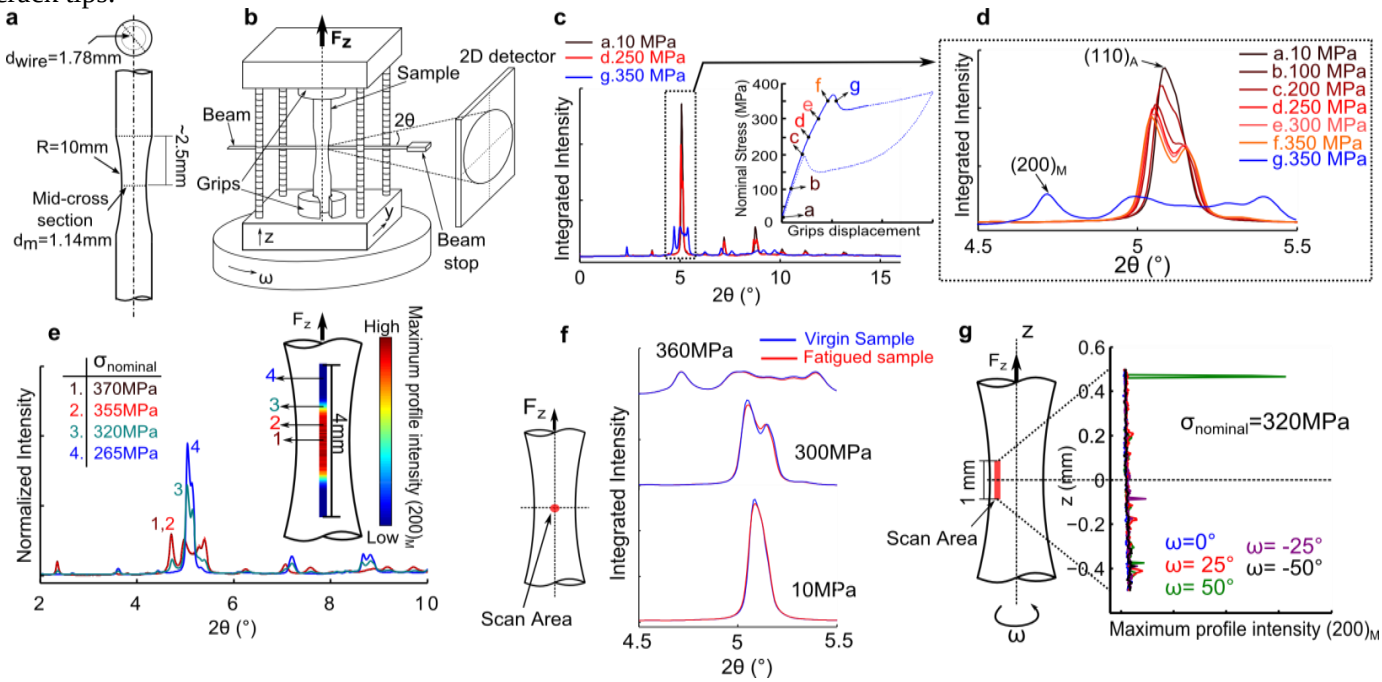

Figure 1. a- Hourglass-shaped samples geometry. **b-** Experimental set up. **c & d-** Diffraction patterns at the mid-cross section of hourglass-shaped samples at different tensile stress magnitudes. **e-** Diffraction pattern evolution with axial stress and a map of initial transformed zone evaluated using maximum profile intensity of $(200)_M$. **f-** Evolution of diffraction patterns of unloaded samples due to fatigue cycling. g- Maximum profile intensity $(200)_M$ evaluated in scanning along the sample axis at different ω angles..

A notched sample was subjected to cyclic loadings while scanning the area around the notch at selected loadings and cycles. As expected, martensite was first detected at the border of the notch (point A in Fig2.a) when nominal stress reached 400MPa, as deduced from the $(110)_A$ peak split into three martensitic peaks including $(200)_M$ (Fig.2b). By mapping the maximum profile intensity of $(200)_M$ we could track the extend of martensite at increasing stress as seen in Fig. 2c.. When stress increased martensite tended to propagate towards the middle of the sample until reaching point B (0.15mm from the border). Further axial deformation made the martensite propagate into two branches. A tensile cycle going up to 530MPa and unloading down to 30MPa resulted in small volume of residual martensite, as evidenced by the distortion of the diffraction pattern at point A (diffraction patterns in Fig. 2d) and $(200)_M$ appearing after unloading around the notch as seen in maps of $(200)_M$ maximum profile intensities in Fig. 2d. These effects evolves during cycling. Nevertheless the evolution rate decreased progressively with cycling being by far largest at first cycles as seen in Fig. 2d on patterns acquired in unloaded state during cycling.

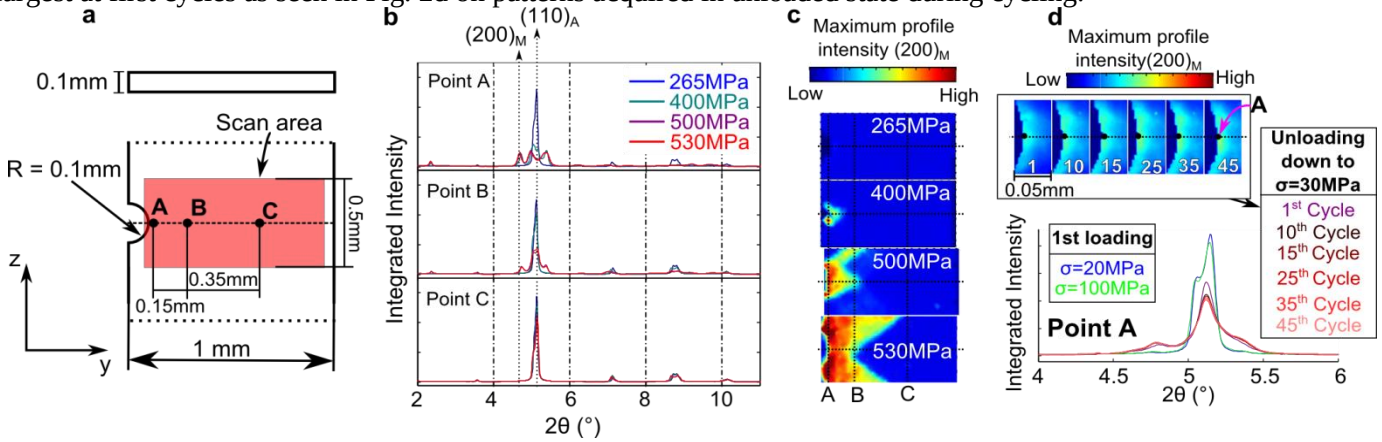

Figure 2. a- Notched ribbon samples geometry. **b-** Diffraction patterns evolution with stress at points A, B and C**. c-**Map of stress-induced martensite at different stresses evaluated using maximum profile intensity of $(200)_M$. **d-** Evolution of diffraction patterns at point A at unloaded state due to superelastic cycling. Maps of residual martensite appearing in unloaded state after superelastic cycling as evaluated using maximum profile intensity of $(200)_M$.

Conclusion

Fatigue loadings near the stress needed to induce martensitic transformation does not cause generalized microstructure distortion on medical-graded NiTi. Nevertheless, damage seems to occur in a smaller scale leading to the formation of cracks. Stress concentration at the crack triggers martensitic transformation at stress magnitudes far below the nominal martensitic transformation stress. It seems that upon further propagation of the martensitic transformation to the bulk induces farther strains, beyond the superelastic limit, to the zone around thus damaging microstructure.

We presented first qualitative results. Data is being further processed with the aim to quantitatively characterise the findings presented in this report. Furthermore, the continuous deformation of just formed martensite in the hourglass-shaped samples will be analysed. As for the experiments with notched samples, 2D stress state preceding the martensitic transformation and at austenite and martensite interfaces will be analysed. Irreversible changes accumulated during cycling in the notch will be quantitatively evaluated.